Incorporating seed orientation in brachytherapy implant reconstruction

Yu Zhou*[a], Ameet K. Jain[b], Gregory S. Chirikjian[c], Gabor Fichtinger[b,c]
[a]Department of Mechanical Engineering, State University of New York at Stony Brook, Stony Brook, NY 11794;
[b]Department of Computer Science, The Johns Hopkins University, Baltimore, MD 21218;
[c]Department of Mechanical Engineering, The Johns Hopkins University, Baltimore, MD 21218.

ABSTRACT

Intra-operative quality assurance and dosimetry optimization in prostate brachytherapy critically depends on the ability of discerning the locations of implanted seeds. Various methods exist for seed matching and reconstruction from multiple segmented C-arm images. Unfortunately, using three or more images makes the problem NP-hard, i.e. no polynomial-time algorithm can provably compute the complete matching. Typically, a statistical analysis of performance is considered sufficient. Hence it is of utmost importance to exploit all the available information in order to minimize the matching and reconstruction errors. Current algorithms use only the information about seed centers, disregarding the information about the orientations and length of seeds. While the latter has little dosimetric impact, it can positively contribute to improving seed matching rate and 3D implant reconstruction accuracy. It can also become critical information when hidden and spuriously segmented seeds need to be matched, where reliable and generic methods are not yet available. Expecting orientation information to be useful in reconstructing large and dense implants, we have developed a method which incorporates seed orientation information into our previously proposed reconstruction algorithm (MARSHAL). Simulation study shows that under normal segmentation errors, when considering seed orientations, implants of 80 to 140 seeds with the density of 2.0- 3.0 seeds/cc give an average matching rate >97% using three-image matching. It is higher than the matching rate of about 96% when considering only seed positions. This means that the information of seed orientations appears to be a valuable additive to fluoroscopy-based brachytherapy implant reconstruction.

Keywords: Prostate brachytherapy, implant reconstruction, seed matching, C-arm fluoroscopy

1. INTRODUCTION

With an approximate annual incidence of 220,000 new cases and 33,000 deaths, prostate cancer continues to be the most common cancer in men in the United States[1]. For several decades, the definitive treatment for low risk prostate cancer was radical prostatectomy or external beam radiation therapy[2], but low dose rate permanent seed brachytherapy (shortly brachytherapy) today can achieve virtually equivalent outcomes[3,4]. The success of brachytherapy (i.e., maximizing its curative force while minimizing its co-morbidity) mainly depends on our ability to tailor the therapeutic dose to the patient's individual anatomy. In contemporary practice, however, implant planning is based on idealistic preplanned seed patterns. 15 years of clinical practice has clearly demonstrated that it is not achievable in the actual human body. According to a comprehensive review by the American Brachytherapy Society[5], the preplanned technique used for permanent prostate brachytherapy has limitations that may be overcome by intraoperative planning. At the same time, the major current limitation of intraoperative planning is the inability to localize the seeds relative to the prostate. There are excellent algorithmic and computational tools available today to optimize a brachytherapy treatment plan intraoperatively, thereby allowing for improved dose coverage. These methods, however, critically require that the exact 3D locations of the implanted seeds are precisely known with respect to the patient's anatomy.

Prostate brachytherapy is almost exclusively performed under transrectal ultrasound imaging (TRUS) guidance. While TRUS provides adequate imaging of the soft tissue anatomy, it does not allow for robust localization of the implanted brachytherapy seeds. Many researchers have tried to segment the seeds from TRUS images by linking seeds with spacers[6], using X-rays to initialize segmentation[7], using vibro-accoustography[8] or transurethral ultrasound[9] as a new imaging modality, or segmenting them directly[10]. But even when meticulously hand-segmented, up to 25% of the seeds

*yuzhou@notes.cc.sunysb.edu; phone (631) 632-8322; fax (631) 632-8544

Medical Imaging 2006: Visualization, Image-Guided Procedures, and Display,
edited by Kevin R. Cleary, Robert L. Galloway, Jr., Proc. of SPIE Vol. 6141, 61411H, (2006)
1605-7422/06/$15 · doi: 10.1117/12.654171

may remain hidden in ultrasound[11]. This necessitates the use of some other imaging method in intraoperative seed localization.

The application of C-arm fluoroscopy in brachytherapy originates when it was first used as a solo guidance modality[12]. Shortly after TRUS emerged as a primary image guidance modality, fluoroscopy became a secondary tool for gross visual observation. Mobile C-arms are ubiquitous in contemporary prostate brachytherapy, with approximately 60% of the practitioners using it for qualitative implant analysis in the operating room[13]. It is considered as the gold standard for intraoperative visualization of brachytherapy seeds. While several groups have published protocols and clinical outcomes favorably supporting C-arm fluoroscopy for intraoperative dosimetric analysis[10,14–22], this technique is yet to become a standard of care across hospitals.

The ability to reconstruct and register the implanted seeds, which are visible in fluoroscopy, to soft tissue anatomy, which is visible in TRUS, intraoperatively would allow us to make immediate provisions for dosimetric deviations from the optimal implant plan. At the same time, quantitative use of fluoroscopy for dosimetric analysis has been hampered by a series of unresolved technical problems. The five major obstacles toward intraoperative dosimetry are: (a) C-arm distortion correction and calibration, (b) C-arm pose tracking, (c) seed segmentation, (d) seed matching and reconstruction, and (e) registration of C-arm to TRUS images.

Significant efforts have been made toward computational fluoroscopy guidance in general surgery, developing various tools for distortion correction and calibration[23,24]. However, C-arms available in most hospitals do not have encoded rotational joints, so one never knows where the fluoro shots are coming from relative to one another. We have addressed this issue by designing a fluoroscope tracking (hence-forth FTRAC) fiducial, which is a radiographic fiducial system creating a unique projection image from each direction[25]. Various methods partially dealing with C-arm calibration in brachytherapy have also been proposed[26–28], while some others have suggested that it is redundant[29].

Attempts have also been made to relate fluoroscopic images to soft tissue anatomy[10,17,30–34]. Nevertheless, further research is merited since existing methods are susceptible to various kinds of errors. We addressed this issue by the use of the FTRAC fiducial[25]. It is capable of not only tracking the C-arm, but also registering the C-arm to TRUS by a predetermined placement.

Methods are available for automatic seed segmentation[15,35–38]. 3D coordinates of the implanted seeds can now be calculated from multiple X-ray images upon resolving the correspondence of seeds. Formalization of the seed-matching problem results in a high complexity search space of the order 10^{150} and 10^{300}, from two and three fluoroscopic images, respectively. Hence previously proposed seed-matching approaches have predominantly been heuristic explorations of the search space, with no theoretical assurance on the accuracy of the answer. The early attempts toward seed matching used three coplanar images (coplanar images are those where the implant and the three X-ray sources are approximately in the same plane)[39-41]. The images were divided into variable width bands, formed by comparing coordinates along the rotation axis. Furthermore, in order to make the bands, it was assumed that the seeds are near the iso-center of the C-arm or at least have similar magnifications in all the images. These methods are prone to calibration errors and become ineffective as the number of seeds increases. These ideas were further extended by accommodating for patients' motion[42], and yet all the seeds could not be reliably reconstructed. Further geometrical constraints were imposed by assuming that some of the seeds are in a straight line[43] or on quadratic curves[44], which is generally not true due to seed migration.

The first step toward mathematical formalization came with the construction of a cost matrix[45], where exhaustive matching gave the lowest cost solution. Though it eliminated extraneous assumptions, it required impractical computational resources. A greedy randomized algorithm, tested with various cost metrics, was suggested to reduce the runtime[46]. This method gives a different output for each run and is typically iterated a few hundred times, choosing the sequentially lowest cost. Though this method might provide an answer close to the correct match, its randomization does not make any claim on the number of iterations required for the final answer. Fast-CARS is another variant[47], which significantly improved the computational complexity, where for each cost matrix an exhaustive match can be performed to obtain the best possible matches. It reduced the run-time from $O((N!)^2)$ to $O((A!)^2)$, where A is the average number of seeds in the band. Though it made the search faster, it still ran in exponential time. For example, if A=10 then the number of computations would still be as high as $O(10^{14})$.

Independently, a set of heuristic rules[16], which attempted to reduce misclassifications, were suggested for seed matching. Simulated annealing[36] was proposed as an alternate technique to reach the global minimum. Another technique[28] was proposed, which optimizes seed positions and camera parameters by generating simulated images and iterating them until they match the observed images. These optimization methods are prone to local minima, and may not be able to recover from them. A statistical simulation of seed reconstruction uncertainty was conducted[48], but did not address the problem of seed matching. CT and MRI based techniques[49,50] were also proposed, but cannot be used intraoperatively, and have poor resolution in the axial direction.

The matching problem is also prevalent in the computer vision community, where 2D points are tracked and reconstructed to compute motion. Researchers have tried to use noniterative greedy algorithms[51], also incorporate spurious and hidden points[52,53]. Occlusion itself has also been a known problem[54]. These algorithms were optimized for a dense set of moving points, while specialized algorithms were used for sparse matchings[55,56], which can also be used in pattern recognition across images[57]. These algorithms are usually catered to achieve real-time performance, as compared to a complete matching, and hence do not appear to be appropriate in a medical application.

In our recent work[59], a new theoretical framework for seed matching has been introduced. The framework tackles issues of optimality, and presents a practical algorithm. Moreover, the framework guarantees a polynomial runtime of $O(N^3)$ on the algorithm, an improvement over previous methods. Seed matching and reconstruction is done by using the Hungarian algorithm (MARSHAL). Simulations and phantom experiments show that MARSHAL is not sensitive to image separation, seed density, the number of seeds, and C-arm calibration, and also robust enough to segmentation, C-arm pose, and distortion. It can reconstruct an implant when three or more images are used, with enough robustness, precision, and speed to support intraoperative dosimetry in prostate brachytherapy. It can also be used as a general purpose correspondence algorithm in many synergistic problems.

In seed matching and reconstruction, it is of utmost importance to exploit all the available information in order to minimize the matching and reconstruction errors. However, current algorithms, including MARSHAL, use only the information about seed centers, disregarding the information about the orientations and length of seeds. While the latter has little dosimetric impact, it can positively contribute to improving seed matching rate and 3D implant reconstruction accuracy. It can also become critical information when hidden and spuriously segmented seeds need to be matched, where reliable and generic methods are not yet available. Expecting orientation information to be useful in reconstructing large and dense implants, in this paper we propose a method which incorporates seed orientation information into MARSHAL.

This paper is organized in the following way. In Sec. 2, we will describe the proposed method which combines the information of seed orientations with that of seed positions. In Sec. 3, we will discuss the simulation study and the results. In Sec. 4, we will conclude our current work and discuss the future work.

2. METHODOLOGY

In this paper we further improve the matching rate of MARSHAL by including the information of seed orientations into the cost matrix. We convert the seed-matching problem to network-flow-based combinatorial optimization. In this formulation, any correspondence of the seeds is represented by an appropriate flow through the network. This formal approach allows better control of the behavior of the algorithm, considering the set of seeds in global optimization instead of local optimization as heuristic rules do.

2.1 A generic network-flow-based formulation

A network flow formulation is created for seed matching problem, where any flow in the network would represent a matching, and the desired solution is the flow with minimum cost. Let N seeds be implanted, and C-arm images I_1, I_2 be acquired. Let s_{ij} be the position of the i^{th} seed in j^{th} image. We construct a directed network as shown in Fig. 1. Sets A and B, each with N nodes, represent the two images I_1 and I_2. While there are no edges within each set, directed edges run from all vertices in set A to all vertices in set B. There are N edges at source S, each edge connecting to a node in A. Similarly each node in B is connected to sink T. The flow originates at S and ends at T, with each edge allowing a flow of value 1 or 0, where 1 means that the edge is selected and 0 means that it is not. The problem is to find a flow in the

network that can achieve a total flow of value N. To have a net flow of N, each edge connecting to either the source or the sink has to support a flow 1. Now by the conservation of flow at each node, every node in set A will have to dispatch a unit flow to some node in set B. Moreover, each node in set B can accept only a unit flow, because any extra flow cannot be passed on to T, and any deficiency would mean that T does not have a total flow of N units. The set of all edges with nonzero flow provide a feasible matching.

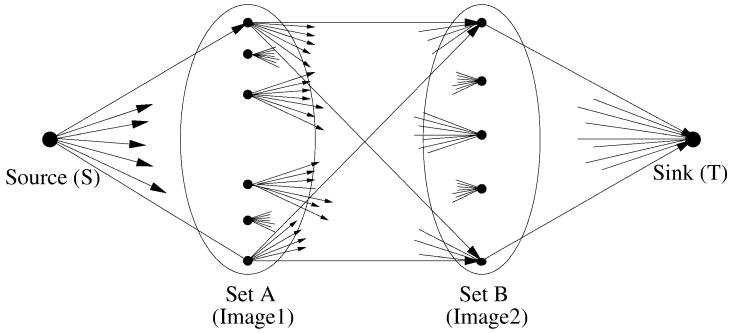

Figure 1: Network flow formulation for the seed matching problem

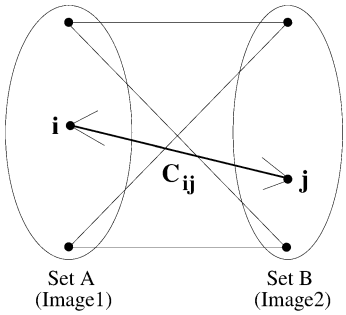

Figure 2: Two-image seed matching as the assignment problem

Under no constraint, the network flow problem has N! solutions, corresponding to N! feasible flows. To obtain the optimal solution, the edge connecting seed s_{i1} to seed s_{j2} is assigned a cost C_{ij}. The cost C_{ij} represents the likelihood of seed s_{i1} matching seed s_{j2}, with the cost being 0 if they match perfectly and ∞ (infinity) if they do not match at all. Any feasible flow has a net cost associated with it, the value of which is $\sum_{i=1}^{n}\sum_{j=1}^{n} C_{ij} f_{ij}$, where f_{ij} is the flow in edge ij, and C_{ij} is the cost of sending a unit flow along that link. Thus the seed matching problem is reduced to finding the flow with minimum cost, and can be written as

$$\min \sum_{i=1}^{N}\sum_{j=1}^{N} C_{ij} f_{ij}, \quad where \quad f_{ij} \in \{0,1\}, \quad \sum_{i=1}^{N} f_{ij} = 1 \,\forall i \quad and \quad \sum_{j=1}^{N} f_{ij} = 1 \,\forall j \cdot \tag{1}$$

The network flow in Fig. 1 can easily be extended to multi-image cases by adding more sets of nodes and directed edges between S and T.

2.2 Seed matching for two and three images

When all the seed locations in the two images are known, the minimum-cost maximum-flow formulation reduces further to the specific problem of minimum-weight matching in bipartite graphs, also known as the assignment problem (Fig. 2). The problem is to find a minimum weight subset of edges such that all the vertices are covered exactly once. The assignment problem is solved in $O(N^3)$ runtime by using the Hungarian algorithm[60–62]. Since the algorithm is well-known, we just give an outline here. The N×N cost matrix C is constructed. The objective is to choose exactly one element from each row and column such that the sum of the elements has the lowest value. Thus, an equivalent matrix having at least one zero in each row and column is obtained by subsequent subtractions using the smallest element in each row and column. This matrix is used to find a selection of zeros such that each row and column has exactly one zero. If it exists, then it provides the minimum-cost matching. If it does not exist, a line covering procedure is used to adjust the matrix and generate zeros in useful locations. The locations of all zeros provide the minimum-weight matching. Thus the Hungarian algorithm provides the matching with the lowest possible cost.

Our previous work has proved that a robust seed matching and reconstruction requires at least three images[59]. In the three-image case, the network flow problem becomes a tripartite matching problem. We proposed a practical solution for matching and reconstruction of brachytherapy seeds using the Hungarian algorithm (MARSHAL)[59]. MARSHAL projects the original tripartite problem into three distinct bipartite problems by the appropriate projection of the costs. Each bipartite problem can be solved in $O(N^3)$ runtime. The solutions of the bipartite matchings are then combined to obtain a solution to the original tripartite problem. A detailed description of MARSHAL algorithm and its theoretical foundation can be found in Ref. 59. A discussion of applying MARSHAL to seed matching from four or more images can also be found there. To avoid redundancy, here we only list the flowchart for MARSHAL (Fig. 3).

2.3 Seed reconstruction

In principle, given three images, the 3D location of a seed can be computed by first defining the equation of the three straight lines that join each projection with its respective X-ray source, and then calculating the intersection point of the three straight lines. However, due to various errors, these straight lines never intersect, forcing us to compute a symbolic 3D intersection point. The symbolic intersection is typically defined as the global minimum of an error function. We have proposed a simple and quick method that minimizes the L_2 norm of Euclidian distance from the intersection point to the lines[59]. Here we assume that for a point P in space, there are m corresponding straight lines (Fig. 4). Line i (l_i) joins the projection of P in image i, p_i, with its X-ray source. The unit directional vector of line i is (a_i ,b_i ,c_i). Then the 3D location of the symbolic intersection point can be calculated as

$$P = (\sum_{i=1}^{m} A_i)^{-1} \sum_{i=1}^{m} A_i p_i \,, \qquad (2)$$

where

$$A_i = \begin{bmatrix} b_i^2 + c_i^2 & -a_i b_i & -a_i c_i \\ -a_i b_i & a_i^2 + c_i^2 & -b_i c_i \\ -a_i c_i & -b_i c_i & a_i^2 + b_i^2 \end{bmatrix}.$$

In Fig. 4, d_i denote the distance from the reconstructed point P to line i.

In principle, 3D seed orientations can also be reconstructed. Given three images, the 3D orientation of a seed can be computed by first defining the three planes that join each projection with its respective X-ray source, and then calculating the intersection line of the three planes. However, due to various errors, these planes never intersect into one straight line in space. So a symbolic intersection becomes necessary. Here we use a simple and quick method to do it (Fig. 5). Here we assume that for a seed S in space, plane i (PL_i) is defined by the projection of S in image i, s_i, with its X-ray source. Since from each pair of planes we can obtain an intersection line, from three planes we can obtain three independent intersection lines. Then we consider the average of the three unit directional vector as the reconstructed 3D orientation of the seed.

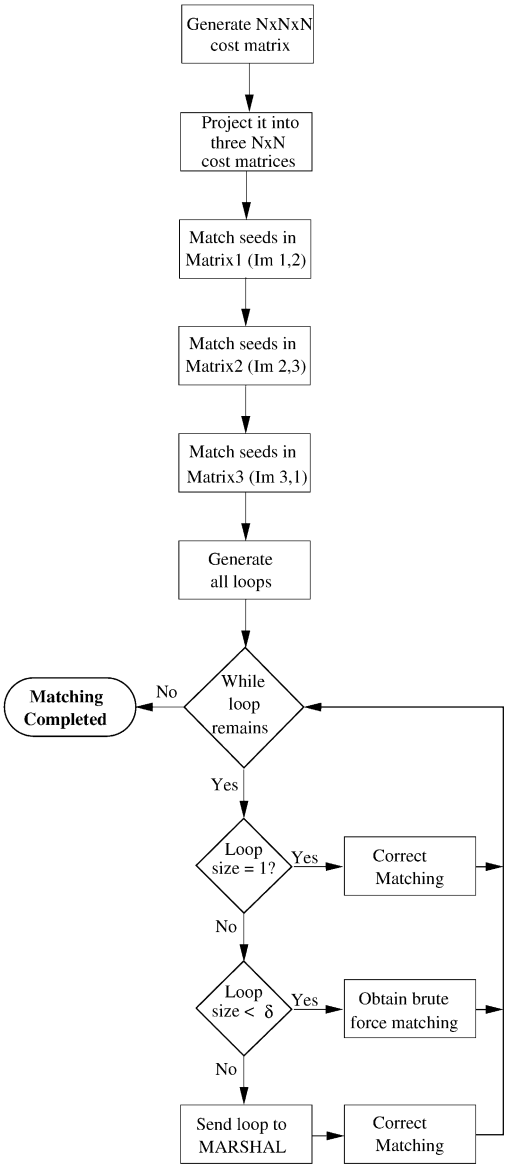

Figure 3: The flowchart of MARSHAL

2.4 Cost metrics

The above discussion shows that a robust seed matching algorithm heavily depends on the performance of the cost metric which constructs the cost matrix in MARSHAL. The seed matching from three images has been reduced to a sequence of bipartite matching. For each bipartite matching problem, we construct a cost matrix in the following way. Given three images, we choose two principal images for this bipartite matching problem. For each pair of seeds in these two images, we reconstruct a 3D seed. Then we project this reconstructed 3D seed to the third image, and find the closest seed projection on the image to this projection based on the cost metric. We reconstruct a 3D seed from those three seed projections. Then we project it back to the three images and calculate the average metric value between each projected seed and the observed seed in each image.

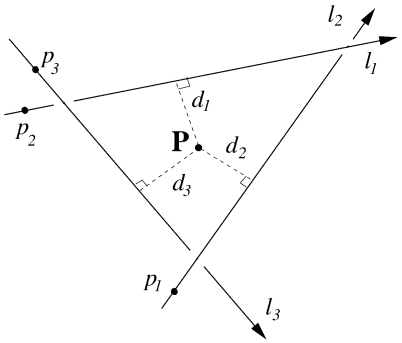

Figure 4: Seed position reconstruction from three images

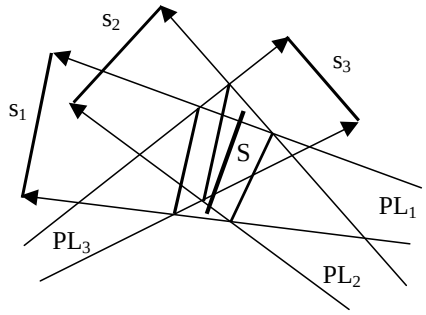

Figure 5: Seed orientation reconstruction from three images

In our previous work, only the positions of seed centers were used to define the cost metric. However, we believe it is of utmost importance to exploit all the available information in order to minimize the matching and reconstruction errors. Although the information about the orientations and length of seeds may have less significant dosimetric impact, it can positively contribute to improving seed matching rate and 3D implant reconstruction accuracy. It can also become critical information when hidden and spuriously segmented seeds need to be matched, where reliable and generic methods are not yet available. In the following, besides the original cost metric used by MARSHAL (M_1), we will introduce several new cost metrics (M_2- M_7) which integrate seed orientation information. Extensive simulation study has been performed to compare the performance among different cost metrics. The results will be reported in Sec.4. Fig. 6 illustrates the seven metrics tested in this study.

2.4.1 M_1 – cost metric without considering seed orientation

The original MARSHAL uses projection error (PE) to define its cost matrix. PE is obtained by projecting the 3D reconstructed point back onto each image and calculating the mean distance between the projected location and the observed location of the seed. In the original MARSHAL, as seen in Fig. 6, the cost metric M_1 is defined as:

$$M_1 = d_c, \tag{3}$$

where, s_p and s_o denote the projected seed and the observed seed respectively, a_p and b_p are the end points of s_p, c_p the center of s_p, a_o and b_o the end points of s_o, c_o the center of s_o, and d_c is the center to center distance between the projected seed and the observed seed.

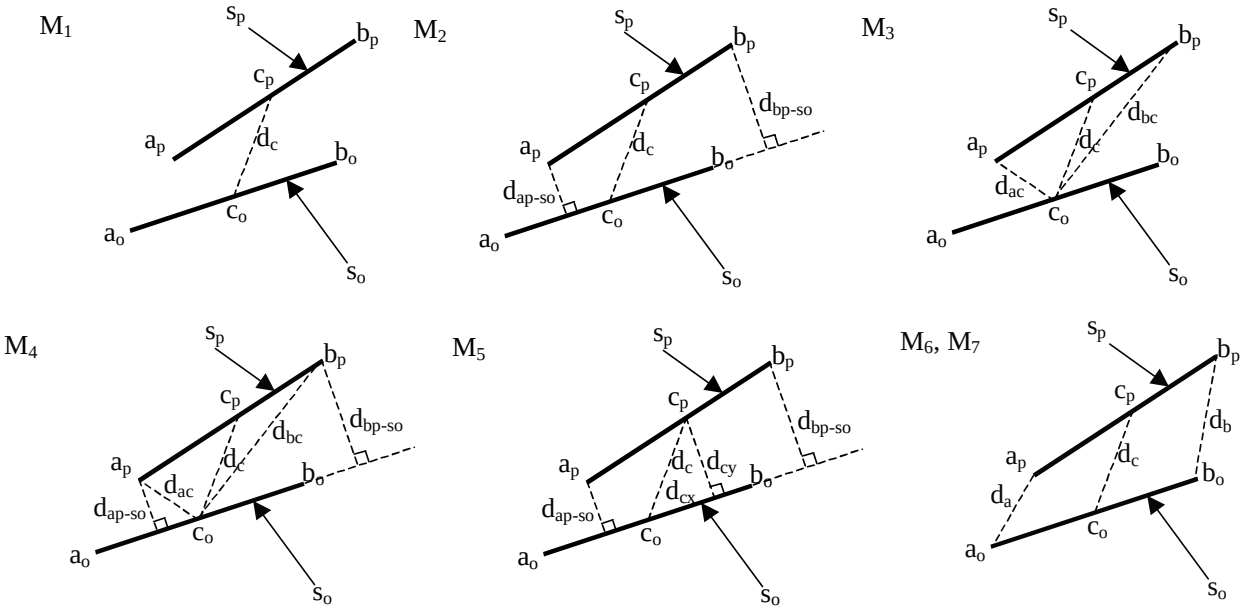

Figure 6: Cost metrics M_1-M_7

Another cost metric (probably the most popular choice) is reconstruction accuracy (RA). RA is obtained by calculating the average distance from the symbolic intersection to each straight line (Fig. 4). It has been proved that PE performs better than RA[59].

2.4.2 M_2 – M_7 Cost metrics considering 2D seed orientation

Combining the information of seed orientations with that of seed positions, we have created a series of cost metrics shown in Fig. 6.

M_2 is defined as

$$M_2 = d_c + d_{ap-so} + d_{bp-so}, \tag{4}$$

where $d_{ap\text{-}so}$ denotes the distance from a_p to s_o, and $d_{bp\text{-}so}$ denotes the distance from b_p to s_o.

M_3 is defined as

$$M_3 = d_c + d_{ac} + d_{bc}, \tag{5}$$

where d_{ac} denotes the distance from a_p to c_o, and d_{bc} denotes the distance from b_p to c_o.

M_4 is defined as

$$M_4 = d_c + d_{ac} + d_{bc} + d_{ap-so} + d_{bp-so}. \tag{6}$$

M_5 is defined as

$$M_5 = d_{cx} + \frac{d_{cy} + d_{ap-so} + d_{bp-so}}{3}, \tag{7}$$

where d_{cx} is the component of d_c along s_o, and d_{cy} is the component of d_c perpendicular to s_o.

M_6 is defined as

$$M_6 = d_c + d_a + d_b, \tag{8}$$

where d_a denotes the distance from a_p to a_o, and d_b denotes the distance from b_p to b_o.

M_7 is defined as

$$M_7 = d_a + d_b. \tag{9}$$

From Fig. 6 and Eq. 4-9, we can see that M_2-M_6 contain not only the center-to-center distance but also the distances related to end points of the seeds. Since the end points define the orientations of the seeds, by including end points into the cost metrics, we have actually incorporated the seed orientation information into the metrics.

2.4.3 M_8- cost metric using threshold for 3D seed orientation

In this case, we define a quantity similar to the RA, the reconstruction accuracy for 3D orientation (RAO). RAO is obtained by calculating the average angular difference from the reconstructed 3D seed orientation to each intersection line obtained from each pair of planes (Fig. 5). In general, for actually matched seeds, the orientations of the three intersection lines are considered not very different from each other. This means that the RAO for actually matched seeds should be small. By setting a threshold for RAO, we define the cost metric M_8 as

$$M_8 = \begin{cases} d_c & RAO \le threshold \\ \infty & RAO > threshold \end{cases}. \tag{10}$$

In this way, we eliminate some potential mismatches early at the stage of constructing cost matrices.

Moreover, we notice that for actually matched seeds, the RA and RAO should be small at the same time. Based on this observation, we propose a simple way to find the optimal threshold for RAO. In order to find the optimal threshold, we choose a range of threshold angles. For each threshold angle in the range, we run MARSHAL with M_8 as the cost metric, and calculate the total RA for the resulting matching. Then we pick the threshold angle with the smallest total RA as the optimal threshold.

3. SIMULATION RESULTS AND DISCUSSION

Extensive simulation study has been done on synthetic images to analyze the performance of MARSHAL under various cost metrics. Matlab program was created to model X-ray imaging. Given C-arm parameters and implant details, it generated synthetic images and exact locations and orientations of seeds in the images. In this paper we use three images to evaluate the correspondences with all the above-mentioned cost metrics. To evaluate the performance on simulated data, we compute the percentage of correct matching. We also study the sensitivity of different cost metrics to segmentation errors, because seed segmentation from the X-ray images is one of the most important sources of error. Here we consider the impact of the segmentation errors in both position and orientation. Random error was modeled following uniform distribution. Therefore, a 1 mm position error means that a maximum error of magnitude 1 mm was added to the positions of the seeds following the uniform distribution. Similarly, a 1° orientation error means that a maximum error of magnitude 1° was added to the orientations of the seeds.

Simulation data sets were generated to simulate different seed densities, prostate volumes and image separation angles. Here we focus on large and dense implants. In our simulation study, the seed density varies from 2.0 seeds/cc to 3.0 seeds/cc, the prostate volume from 40cc to 45cc, and image separation angle from 15° to 20°. So the total number of seeds is from 80 to 140. To test the impact of segmentation errors on the cost metrics, we vary the segmentation error in position from 0 mm to 1.5 mm, and the segmentation error in orientation from 0° to 30°. The averaged results are displayed in Tables 1 and 2. The general trend can be seen in Fig. 7 and 8. When we test the metrics with orientation segmentation error, we fix the position segmentation error as 0.75 mm; when we test the metrics with position segmentation error, we fix the orientation error as 9°. This is because they are close to the segmentation errors in practice.

Matching rate (%)			Orientation segmentation errors										
			0°	3°	6°	9°	12°	15°	18°	21°	24°	27°	30°
Cost Metrics	M_1	Avg.	96.3%	96.3%	96.3%	96.3%	96.3%	96.3%	96.3%	96.3%	96.3%	96.3%	96.3%
		STD	2.3%	2.3%	2.3%	2.3%	2.3%	2.3%	2.3%	2.3%	2.3%	2.3%	2.3%
	M_2	Avg.	98.4%	98.1%	97.6%	96.2%	93.8%	93.2%	91.8%	91.5%	91.0%	90.3%	90.8%
		STD	1.8%	1.8%	2.2%	2.7%	3.7%	3.0%	3.8%	3.3%	4.0%	4.3%	4.1%
	M_3	Avg.	88.2%	91.5%	93.5%	93.1%	92.4%	92.9%	91.8%	91.8%	92.6%	91.7%	92.0%
		STD	5.7%	3.7%	4.0%	4.0%	3.1%	3.4%	3.6%	4.1%	3.4%	3.9%	3.7%
	M_4	Avg.	96.3%	96.9%	96.4%	95.1%	92.9%	92.8%	90.7%	90.7%	90.6%	89.3%	90.7%
		STD	2.6%	2.2%	2.5%	3.2%	3.8%	2.8%	3.8%	3.9%	3.1%	4.3%	3.6%
	M_5	Avg.	98.1%	98.0%	97.9%	97.1%	95.5%	95.7%	95.1%	94.0%	94.8%	94.0%	94.6%
		STD	1.8%	1.8%	2.1%	2.1%	3.0%	2.9%	3.0%	3.0%	2.8%	3.6%	3.4%
	M_6	Avg.	98.4%	98.2%	98.1%	97.2%	95.4%	94.6%	93.5%	92.2%	93.3%	91.6%	92.8%
		STD	1.6%	1.8%	1.9%	2.2%	3.0%	2.9%	3.5%	3.7%	3.5%	3.8%	3.5%
	M_7	Avg.	98.6%	98.4%	98.0%	96.7%	93.8%	92.5%	90.8%	89.5%	89.7%	87.9%	88.0%
		STD	1.6%	1.7%	2.0%	2.4%	3.8%	3.2%	4.2%	3.6%	3.9%	4.9%	4.7%
	M_8	Avg.	96.5%	96.4%	96.5%	96.6%	96.5%	96.6%	96.6%	96.6%	96.3%	96.4%	96.3%
		STD	2.2%	2.2%	2.2%	2.2%	2.2%	2.2%	2.2%	2.2%	2.2%	2.3%	2.3%

Table 1: Matching rate from various cost metrics under different orientation segmentation errors (with a fixed position segmentation error of 0.75 mm)

Reconstruction error (mm)			Orientation segmentation errors										
			0°	3°	6°	9°	12°	15°	18°	21°	24°	27°	30°
Cost Metrics	M_1	All	0.50	0.50	0.50	0.50	0.50	0.50	0.50	0.50	0.50	0.50	0.50
		Mat.	0.49	0.49	0.49	0.49	0.49	0.49	0.49	0.49	0.49	0.49	0.49
		Mis.	0.65	0.65	0.65	0.65	0.65	0.65	0.65	0.65	0.65	0.65	0.65
	M_2	All	0.50	0.50	0.50	0.52	0.55	0.55	0.55	0.59	0.66	0.62	0.65
		Mat.	0.49	0.49	0.49	0.49	0.49	0.49	0.49	0.50	0.51	0.50	0.51
		Mis.	0.50	0.57	0.74	0.98	1.10	1.15	1.17	1.40	1.61	1.43	1.56
	M_3	All	0.76	0.59	0.57	0.60	0.54	0.53	0.58	0.55	0.54	0.56	0.56
		Mat.	0.52	0.50	0.50	0.51	0.49	0.49	0.51	0.49	0.49	0.49	0.49
		Mis.	1.71	1.24	1.08	1.15	1.06	0.96	1.21	1.12	1.05	1.13	1.10
	M_4	All	0.52	0.50	0.51	0.54	0.54	0.54	0.58	0.57	0.62	0.61	0.59
		Mat.	0.49	0.49	0.49	0.49	0.49	0.49	0.49	0.49	0.50	0.49	0.50
		Mis.	0.92	0.66	0.87	1.13	1.15	1.12	1.31	1.20	1.58	1.45	1.24
	M_5	All	0.50	0.50	0.50	0.50	0.51	0.51	0.52	0.52	0.51	0.53	0.51
		Mat.	0.49	0.49	0.49	0.49	0.49	0.49	0.49	0.49	0.49	0.49	0.49
		Mis.	0.63	0.52	0.56	0.66	0.76	0.80	0.88	0.86	0.79	1.00	0.69
	M_6	All	0.50	0.50	0.50	0.50	0.51	0.52	0.52	0.55	0.57	0.59	0.55
		Mat.	0.49	0.49	0.49	0.49	0.49	0.49	0.49	0.50	0.50	0.50	0.49
		Mis.	0.53	0.49	0.50	0.64	0.78	0.92	0.93	1.11	1.11	1.40	1.09
	M_7	All	0.50	0.50	0.50	0.51	0.53	0.56	0.56	0.60	0.65	0.70	0.72
		Mat.	0.49	0.49	0.49	0.49	0.49	0.49	0.49	0.50	0.50	0.50	0.51
		Mis.	0.52	0.48	0.58	0.74	0.91	1.27	1.28	1.30	1.58	1.76	1.94
	M_8	All	0.50	0.50	0.50	0.50	0.50	0.50	0.50	0.50	0.50	0.50	0.50
		Mat.	0.49	0.49	0.49	0.49	0.49	0.49	0.49	0.49	0.49	0.49	0.49
		Mis.	0.65	0.65	0.64	0.64	0.65	0.64	0.64	0.65	0.72	0.65	0.65

Table 2: Average reconstruction error from various cost metrics under different orientation segmentation errors (with a fixed position segmentation error of 0.75 mm). “Mat.” stands for matched seeds, “Mis.” stands for mismatched seeds.

Matching rate (%)			Position segmentation errors (mm)						
			0	0.25	0.5	0.75	1.0	1.25	1.5
Cost Metrics	M_1	Avg.	100.0%	99.5%	98.5%	96.0%	92.5%	86.7%	76.2%
		STD	0.0%	0.9%	1.7%	2.2%	4.0%	4.9%	6.1%
	M_2	Avg.	99.3%	98.8%	98.1%	96.6%	93.6%	87.5%	78.4%
		STD	0.9%	1.2%	1.9%	2.4%	3.8%	4.9%	7.7%
	M_3	Avg.	98.5%	97.4%	95.7%	93.5%	90.2%	83.3%	73.6%
		STD	1.4%	2.0%	2.4%	3.5%	4.0%	6.6%	7.9%
	M_4	Avg.	99.0%	98.5%	97.5%	95.8%	92.5%	87.1%	77.6%
		STD	1.3%	1.6%	1.7%	3.1%	3.7%	6.0%	7.4%
	M_5	Avg.	99.8%	99.4%	98.6%	97.1%	94.2%	89.6%	80.7%
		STD	0.3%	1.0%	1.6%	2.2%	3.6%	4.7%	6.3%
	M_6	Avg.	99.6%	99.0%	98.5%	97.2%	95.1%	90.1%	82.1%
		STD	0.7%	1.1%	1.6%	2.4%	3.1%	5.2%	6.4%
	M_7	Avg.	98.8%	98.6%	97.9%	96.8%	94.8%	90.7%	83.1%
		STD	1.3%	1.3%	1.9%	2.4%	3.3%	5.2%	6.2%
	M_8	Avg.	100.0%	99.5%	98.6%	96.2%	92.9%	88.2%	78.3%
		STD	0.0%	0.9%	1.5%	2.3%	3.9%	4.9%	5.6%

Table 3: Matching rate of various cost metrics under different position segmentation errors (with a fixed orientation segmentation error of 9°)

Reconstruction error (mm)			Position segmentation errors (mm)						
			0	0.25	0.5	0.75	1.0	1.25	1.5
Cost Metrics	M_1	All	0.00	0.16	0.32	0.50	0.71	1.21	2.01
		Mat.	0.00	0.16	0.32	0.48	0.63	0.84	1.06
		Mis.	0.00	0.08	0.38	0.82	1.44	2.94	4.06
	M_2	All	0.01	0.17	0.32	0.50	0.72	1.20	2.07
		Mat.	0.00	0.16	0.32	0.48	0.63	0.83	1.07
		Mis.	0.14	0.25	0.39	0.80	1.61	3.26	4.33
	M_3	All	0.01	0.17	0.34	0.53	0.82	1.48	2.32
		Mat.	0.00	0.16	0.32	0.48	0.66	0.85	1.13
		Mis.	0.29	0.45	0.62	1.06	1.85	3.65	4.34
	M_4	All	0.01	0.17	0.34	0.51	0.74	1.32	2.09
		Mat.	0.00	0.16	0.32	0.48	0.64	0.84	1.09
		Mis.	0.26	0.33	0.73	0.91	1.58	3.45	4.23
	M_5	All	0.00	0.16	0.32	0.50	0.69	1.10	1.78
		Mat.	0.00	0.16	0.32	0.48	0.63	0.81	1.04
		Mis.	0.04	0.10	0.36	0.77	1.30	2.77	3.63
	M_6	All	0.00	0.16	0.32	0.49	0.67	1.07	1.69
		Mat.	0.00	0.16	0.31	0.48	0.63	0.81	1.01
		Mis.	0.09	0.20	0.38	0.69	1.22	2.49	3.50
	M_7	All	0.01	0.17	0.33	0.50	0.67	1.00	1.58
		Mat.	0.00	0.16	0.32	0.48	0.63	0.80	1.02
		Mis.	0.33	0.36	0.56	0.87	1.28	2.19	3.13
	M_8	All	0.00	0.16	0.32	0.50	0.70	1.08	1.79
		Mat.	0.00	0.16	0.32	0.48	0.63	0.82	1.05
		Mis.	0.00	0.07	0.38	0.82	1.43	2.42	3.53

Table 4: Average reconstruction error from various cost metrics under different position segmentation errors (with a fixed orientation segmentation error of 9°). "Mat." stands for matched seeds, "Mis." stands for mismatched seeds.

From the tables and figures, we can see two clear trends:

1. When the position segmentation error increases, the matching rate based on each cost metric decreases monotonically. This is because all the cost metrics we discussed depend on the distance between the projected seeds and the observed seeds. The increase in position segmentation error will cause the difference between the metric values of actually matched seeds and those of actually unmatched seeds decrease.
2. When the orientation segmentation error increase, the matching rate of the cost metrics considering orientation decreases. This is because these cost metrics depend on reasonably accurate 2D orientation information. The increase in orientation segmentation error will cause the difference between the metric values of actually matched seed and those of actually unmatched seeds decrease.

Moreover, if we use M_1 (the cost metric without considering seed orientation) as a criterion, M_8 (the cost metric using threshold for 3D seed orientation) always give us a matching rate equal to or slightly greater than that of M_1. This is because M_8 is built upon M_1 with a threshold. It guarantees that M_8 performs at least as well as M_1. However, it also means that no substantial improvement over M_1 can be obtained from M_8. The data show that the matching rate of M_3 is always below that of M_1. The matching rate of M_4 drops below that of M_1 right after the orientation segmentation error hits 6°, while its sensitivity to the position segmentation error is about same as M_1. Therefore, M_3, M_4 and M_8 are not recommended.

The data also show that the matching rates of M_2, M_5, M_6 and M_7 are higher than that of M_1 when the orientation segmentation error is lower than 9°. Among them M_5 and M_6 are better than M_2 and M_7. When the orientation segmentation error is equal to 9°, M_5 and M_6 give the matching rates greater than 97% while M_2 and M_7 are close to M_1, about 96%. Meanwhile, the standard deviation of the matching rates of M_5 and M_6 are also slightly smaller than that of M_1. M_5 and M_6 also give the best matching rates when the position segmentation error is close to the practice (0.75mm). At the same time, the average reconstruction errors of mismatched seeds from M_5 and M_6 are about same as or slightly

lower than that of M_1 at the segmentation errors of 9° and 0.75mm. Therefore M_5 and M_6 are the best cost metrics we have. They can be used to robustly match and reconstruct seeds under normal segmentation errors. It also means that combining seed orientation information into the cost metric does result in certain improvement in the performance of the algorithm.

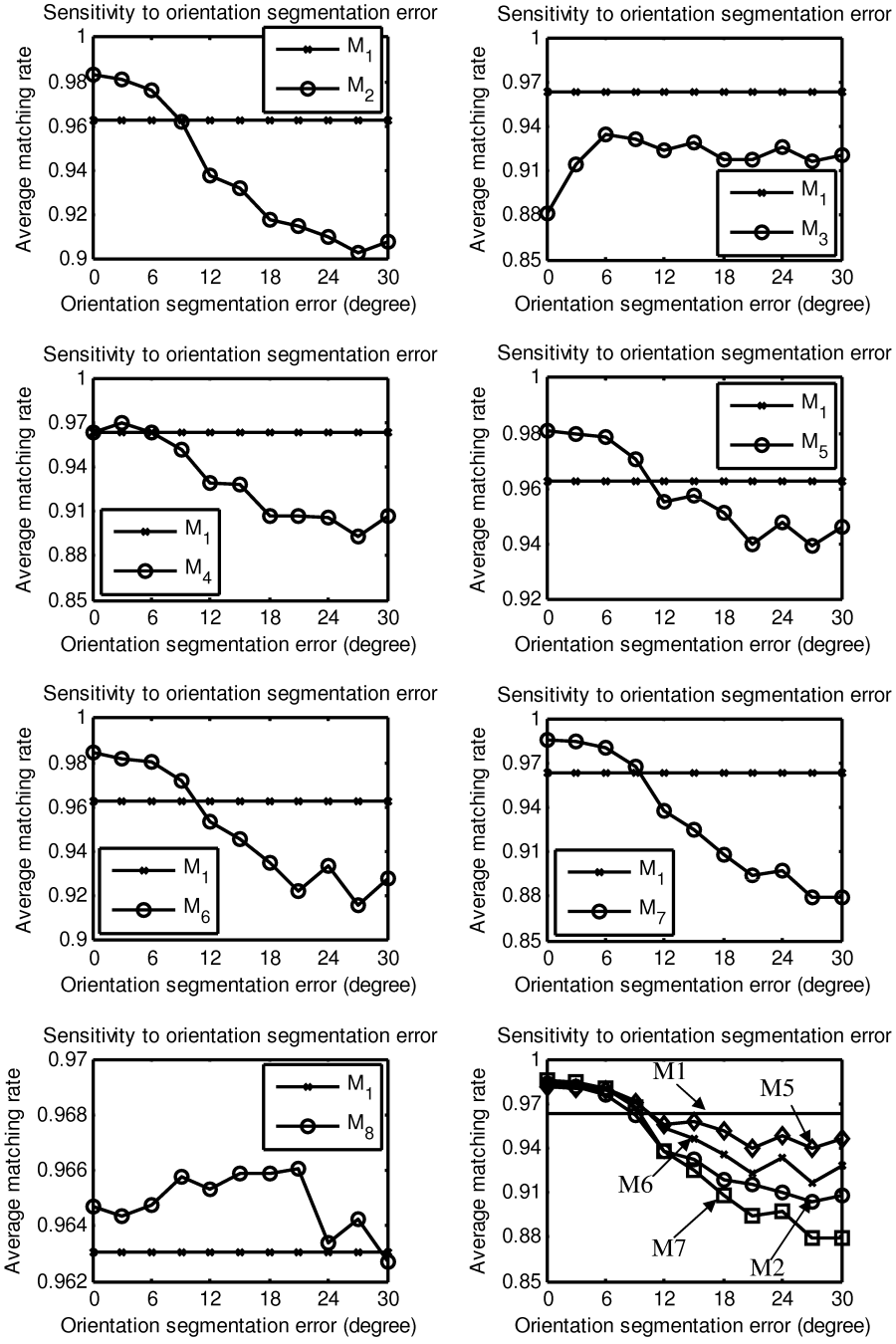

Figure 7: Sensitivity of cost metrics to orientation segmentation error

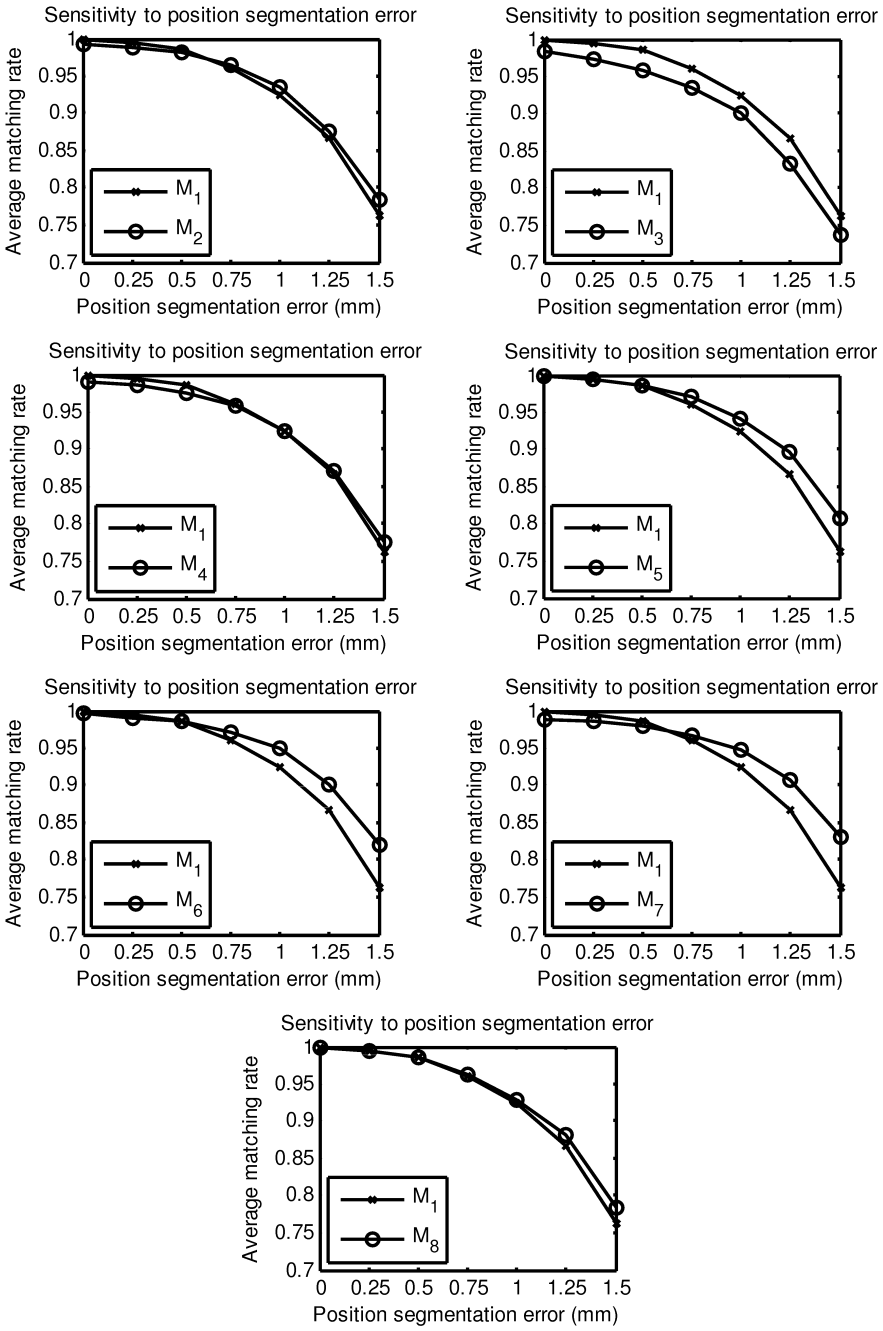

Figure 8: Sensitivity of cost metrics to position segmentation error

4. CONCLUSIONS AND FUTURE WORK

In this paper, we have extended our previously proposed quasi-polynomial time algorithm (MARSHAL) to combine the information of seed orientations into matching procedure. Simulation results show that the cost metrics considering seed orientation can further improve the matching rate of MARSHAL, and robust to certain amount of seed segmentation errors in both position and orientation.

An underlying assumption of MARSHAL is that all the seeds are segmented and their 2D positions and orientations are known. In reality, however, some seeds always remain hidden, and some are segmented spuriously[35,63,64]. In a parallel work[63], we extended MARSHAL to deal with hidden seeds. In phantom study, we managed to recover >96% seeds from three images and >99% from four images, and the algorithm was robust to segmentation error up to 1 mm and hidden seed rate up to 8%. While the matching rate was excellent, the reconstruction error for mismatched seeds remained 3-8mm. In this paper, Sec. 3 shows that under average segmentation errors, cost metrics that utilize seed orientation significantly lower the reconstruction error for mismatched seeds, generally to less than 1mm.

We conjecture that combining these new cost metrics in our hidden seed recovery method[63] will result in superior seed matching rate and low reconstruction error for both matched and unmatched seeds, and thereby yield a clinically applicable solution.

ACKNOWLEDGEMENTS

This work has been supported by NIH 1R43CA099374-01, NSF EEC-9731478 and DOD PC050170.

REFERENCES

1. A. Jemal, "Cancer statistics," Ca-Cancer J. Clin. **54**(1), 8–29, 2004.
2. R. Peschel and J. Colberg, "Surgery, brachytherapy, and external-beam radiotherapy for early prostate cancer," Lancet Oncol. **4**, 233–241, 2003.
3. J. Blasko, T. Mate, J. Sylvester, P. Grimm, and W. Cavanagh, "Brachytherapy for carcinoma of the prostate: Techniques, patient selection, and clinical outcomes," Semin. Radiat. Oncol. **12**, 81–94, 2002.
4. G. Merrick, W. Butler, J. Lief, and A. Dorsey, "Is brachytherapy comparable with radical prostatectomy and external-beam radiation for clinically localized prostate cancer?," Tech. Urol. **7**, 12–19, 2001.
5. S. Nag, J. Ciezki, R. Cormack, S. Doggett, K. DeWyngaert, G. Edmundson, R. Stock, N. Stone, Y. Yu, and M. Zelefsky, "Intraoperative planning and evaluation of permanent prostate brachytherapy: Report of the American Brachytherapy Society," Int. J. Radiat. Oncol., Biol., Phys. **51**, 1422–1430, 2001.
6. J. Xue, E. Gressen, and T. Jefferson, "Feasibility of trus-based prostate post-implant dosimetry," AAPM Annual Meeting, July 2004, Poster.
7. V. A. Dumane, M. Zaider, G. N. Cohen, and W. M. F. Worman, "Combined ultrasound-fluoroscopy approach to the intraoperative detection of seeds in prostate brachytherapy," ASTRO Annual Meeting, Poster, Oct 3–7 2004.
8. F. Mitri, P. Trompette, and J. Chapelon, "Improving the use of vibroacoustography for brachytherapy metal seed imaging: A feasibility study," IEEE Trans. Med. Imaging **23**, 1–6, 2004.
9. D. Holmes, B. Davis, C. Bruce, and R. Robb, "3d visualization, analysis, and treatment of the prostate using trans-urethral ultrasound," Comput. Med. Imaging Graph. **27**, 339–349, 2003.
10. D. French, J. Morris, M. Keyes, and S. E. Salcudean, "Real-time dosimetry for prostate brachytherapy using trus and fluoroscopy," MICCAI 2004, 983–991.
11. B. Han, K. Wallner, G. Merrick, W. Butler, S. Sutlief, and J. Sylvester, "Prostate brachytherapy seed identification on post-implant trus images," Med. Phys. **30**, 898–900, 2003.
12. P. Kumar, R. Good, B. Epstein, M. Hussain, and F. Bartone, "Fluoroscopy guided transperineal percutaneous permanent 125iodine implantation of prostate cancer," Radiat. Med. **3**, 161–167, 1985.
13. B. Prestidge, J. Prete, T. Buchholz, J. Friedland, R. Stock, P. Grimm, and W. Bice, "A survey of current clinical practice of permanent prostate brachytherapy in the United States," Int. J. Radiat. Oncol., Biol., Phys. **15**, 461–465, 1998.
14. P. Ravindran, C. Lewis, J. Alphonsi, P. Lindsay, and D. D'Souza, "A c-arm based intra-operative dosimetry system for trans-rectal ultrasound guided prostate implant with 125I seeds," in Proceedings of the 14th International Conference on the Use of Computers in Radiation Therapy, 2004.
15. D. Todor, M. Zaider, G. Cohen, M. Worman, and M. Zelefsky, "Intraoperative dynamic dosimetry for prostate implants," Phys. Med. Biol. **48**, 1153–1171, 2003.
16. D. Todor, G. Cohen, H. Amols, and M. Zaider, "Operator-free, film-based 3d seed reconstruction in brachytherapy," Phys. Med. Biol. **47**, 2031–2048, 2002.
17. L. Gong, P. Cho, B. Han, K. Wallner, S. Sutlief, S. Pathak, D. Haynor, and Y. Kim, "Ultrasonography and fluoroscopic fusion for prostate brachytherapy dosimetry," Int. J. Radiat. Oncol., Biol., Phys. **1**, 1322– 1330, 2002.

18. G. Grado, T. Larson, C. Balch, M. Grado, J. Collins, J. Kriegshauser, G. Swanson, R. Navickis, and M. Wilkes, "Actuarial disease-free survival after prostate cancer brachytherapy using interactive techniques with biplane ultrasound and fluoroscopic guidance," Int. J. Radiat. Oncol., Biol., Phys. **1**, 289–299, 1998.
19. G. Merrick, W. Butler, A. Dorsey, and H. Walbert, "Prostatic conformal brachytherapy: 125i/103pd postoperative dosimetric analysis," Radiat. Oncol. Invest. **5**, 305–313, 1997.
20. D. Nori and J. Moni, "Current issues in techniques of prostate brachytherapy," Semin Surg. Oncol. **13**, 444–453, 1997.
21. S. Nag, D. Scaperoth, R. Badalament, S. Hall, and J. Burgers, "Transperineal palladium 103 prostate brachytherapy: Analysis of morbidity and seed migration," Urology **45**, 87–92, 1995.
22. K. Wallner, S. Chiu-Tsao, J. Roy, V. Arterbery, W. Whitmore, S. Jain, B. Minsky, P. Russo, and Z. Fuks, "An improved method for computerized tomography-planned transperineal 125iodine prostate implants," J. Urol. **146**, 90–95, 1991.
23. R. Hofstetter, M. Slomczykowski, M. Sati, and L. Nolte, "Fluoroscopy as an imaging means for computer-assisted surgical navigation," Comput. Aided Surg. **4**, 65–76, 1999.
24. J. Yao, R. H. Taylor, R. P. Goldberg, R. Kumar, A. Bzostek, V. R. Van, P. Kazanzides, and A. Gueziec, "A c-arm fluoroscopy-guided progressive cut refinement strategy using a surgical robot," Comput. Aided Surg. **5**, 373–390, 2000.
25. A. Jain, T. Mustufa, Y. Zhou, E. C. Burdette, G. Chirikjian, and G. Fichtinger, "A robust fluoroscope tracking (ftrac) fiducial," Med. Phys. **32**, 3185–3198, 2005.
26. A. Fung, "C-arm imaging for brachytherapy source reconstruction: Geometrical accuracy," Med. Phys. **29**, 724–726, 2002.
27. S. Narayanan and P. Cho, "3d seed reconstruction from unknown imaging geometry," in Proceedings of the 14th International Conference on the Use of Computers in Radiation Therapy, 2004, 762–765.
28. M. Murphy and D. Todor, "Demonstration of a forward iterative method to reconstruct brachytherapy seed configurations from x-ray projections," Phys. Med. Biol. **50**, 2715–2737, 2005.
29. A. Jain, R. Kyon, Y. Zhou and G. Fichtinger, "C-arm calibration—Is it really necessary?," Medical Image Computing and Computer Assisted Interventions (MICCAI), 2005.
30. K. Wallner, J. Roy, M. Zelefsky, Z. Fuks, and L. Harrison, "Fluoroscopic visualization of the prostatic urethra to guide transperineal prostate implantation," Int. J. Radiat. Oncol., Biol., Phys. **1**, 863–867, 1994.
31. P. Roberson, V. Narayana, D. McShan, R. Winfield, and P. McLaughlin, "Source placement error for permanent implant of the prostate," Med. Phys. **24**, 251–257, 1997.
32. M. Baird, R. Holt, and T. Selby, "Improvement of transperineal implant dosimetry by intraoperative cystoscopic confirmation of prostate anatomy," J. Urol. **164**, 406–410, 2000.
33. L. Archambault, L. Beaulieu, and D. Tubic, "Automatic post-implant needle reconstruction algorithm to characterize and improve implant robustness analyses," Med. Phys. **30**, 2897–2903, 2003.
34. M. Zhang, M. Zaider, M. Worman, and G. Cohen, "On the question of 3d seed reconstruction in prostate brachytherapy: The determination of x-ray source and film locations," Phys. Med. Biol. **49**, N335–345, 2004.
35. Y. Su, B. Davis, M. Herman, and R. Ra, "Prostate brachytherapy seed localization by analysis of multiple projections: Identifying and addressing the seed overlap problem," Med. Phys. **31**, 1277–1287, 2004.
36. D. Tubic, A. Zaccarin, J. Pouliot, and L. Beaulieu, "Automated seed detection and three-dimensional reconstruction. II. Reconstruction of permanent prostate implants using simulated annealing," Med. Phys. **28**, 2272–2279, 2001.
37. S. Lam, P. Cho, and R. Marks, "Prostate brachytherapy seed segmentation using spoke transform," Proc. SPIE **4322**, 1490–1500, 2001.
38. P. Cho, "Computerized segmentation of clustered seeds in prostate brachytherapy," International Conference on the Use of Computers in Radiation Therapy, 2000, 105–107.
39. H. Amols and I. Rosen, "A three-film technique for reconstruction of radioactive seed implants," Med. Phys. **8**, 210–214, 1981.
40. P. Biggs and D. Kelley, "Geometric reconstruction of seed implants using a three-film technique," Med. Phys. **10**, 701–704, 1983.
41. M. Rosenthal and R. Nath, "An automatic seed identification technique for interstitial implants using three isocentric radiographs," Med. Phys. **10**, 475–479, 1983.
42. M. Altschuler, P. Findlay, and R. Epperson, "Rapid accurate, threedimensional location of multiple sees in implant radiotherapy treatment planning," Phys. Med. Biol. **28**, 1305–1308, 1983.

43. D. Jackson, “An automatic method for localizing radioactive seeds in implant dosimetry,” Med. Phys. **10**, 370–372, 1983.
44. S. Li, G. Chen, C. Pelizzari, C. Reft, J. Roeske, and Y. Lu, “A new source localization algorithm with no requirement of one-to-one source correspondence between biplane radiographs,” Med. Phys. **23**, 921–927, 1996.
45. R. L. Siddon and L. M. Chin, “Two-film brachytherapy reconstruction algorithm,” Med. Phys. **12**, 77–83, 1985.
46. M. Altschuler and A. Kassaee, “Automated matching of corresponding seed images of three simulator radiographs to allow 3d triangulation of implanted seeds,” Phys. Med. Biol. **42**, 293–302, 1997.
47. S. Narayanan, P. Cho, and R. Marks, “Fast cross-projection algorithm for reconstruction of seeds in prostate brachytherapy,” Med. Phys. **29**, 1572–1579, 2002.
48. K. Thornton, “Prostate brachytherapy seed localization by fluoroscopy/ ultrasound fusion: Algorithms and analysis,” AAPM Annual Meeting, July 2004.
49. H. Liu, G. Cheng, Y. Yu, R. Brasacchio, D. Rubens, J. Strang, L. Liao, and E. Messing, “Automatic localization of implanted seeds from postimplant ct images,” Phys. Med. Biol. **48**, 1191–1203, 2003.
50. D. Dubois, W. J. Bice, and B. Prestige, “Ct and mri derived source localization error in a custom prostate phantom using automated image coregistration,” Med. Phys. **28**, 2280–2284, 2001.
51. K. Shafique and M. Shah, “A non-iterative greedy algorithm for multiframe point correspondence,” ICCV, 2003.
52. C. J. Veenman, M. J. T. Reinders, and E. Backer, “Resolving motion correspondence for densely moving points,” IEEE Trans. Pattern Anal. Mach. Intell. **23**, 54–72, 2001.
53. C. Veenman, M. Reinders, and E. Backer, “Establishing motion correspondence using extended temporal scope,” Artificial Intelligience **145**, 227–243, 2003.
54. V. Salari and I. Sethi, “Feature point correspondence in the presence of occlusion,” Pattern Anal. Machine Intell. **12**, 87–91, 1990.
55. Y. Cheng, R. Collins, A. Hanson, and E. Riseman, “Triangulation without correspondences,” ARPA94, 1994, II:993–1000.
56. Y. Cheng, V. Wu, R. Collins, A. Hanson, and E. Riseman, “Maximumweight bipartite matching technique and its application in image feature matching,” 1996.
57. *Artificial Intelligence: A Modern Approach*, Prentice Hall Series in Artificial Intelligence, edited by S. Russell and P. Norvig, 2nd ed..
58. T. H. Cormen, C. E. Leiserson, and R. Rivest, *Introduction to Algorithms* 2nd ed. MIT Press, 1990.
59. A. K. Jain, Y. Zhou, T. Mustufa, E. C. Burdette, G. S. Chirikjian, G. Fichtinger, “Matching and reconstruction of brachytherapy seeds using the Hungarian algorithm (MARSHAL)”, Med. Phys. **32** (11), 3475-3492, 2005.
60. R. K. Ahuja, T. L. Magnanti, and J. B. Orlin, *Network Flows: Theory, Algorithms, and Applications*, 1st ed. Prentice Hall, Englewood Cliffs, NJ, 1993.
61. H. W. Kuhn, “The Hungarian method for the assignment problem,” Naval Res. Logistics Quart. **2**, 83–97, 1955.
62. C. H. Papadimitriou and K. Steiglitz, *Combinatorial Optimization: Algorithms and Complexity*, Prentice-Hall, Englewood Cliffs, NJ, 1982.
63. R. C. Kon, A. Jain and G. Fichtinger, “Hidden seed reconstruction from C-arm images in brachytherapy”, ISBI 2006, Washington D.C., April 2006 (accepted).
64. S. Narayanan, P. S. Cho and R. J. Marks, “Three-dimensional seed reconstruction from an incomplete data set for prostate brachytherapy”, Phys. Med. Biol. **49** (15): 3483-3494, 2004.